Molecular Therapy
Nucleic Acids
Original Article

Engineered AAV capsid transport mutants overcome transduction deficiencies in the aged CNS

Ivette M. Sandoval,[1] Christy M. Kelley,[1] Luis Daniel Bernal-Conde,[1] Kathy Steece-Collier,[2] David J. Marmion,[1] Marcus Davidsson,[1] Sean M. Crosson,[3] Sanford L. Boye,[4] Shannon E. Boye,[3] and Fredric P. Manfredsson[1]

[1]Parkinson's Disease Research Unit, Department of Translational Neuroscience, Barrow Neurological Institute, Phoenix, AZ 85013, USA; [2]Department of Translational Neuroscience, Michigan State University College of Human Medicine, Grand Rapids, MI 49506, USA; [3]Division of Cellular and Molecular Therapy, Department of Pediatrics, University of Florida, Gainesville, FL 32610, USA; [4]Powell Gene Therapy Center, Department of Pediatrics, University of Florida, Gainesville, FL 32610, USA

Adeno-associated virus (AAV)-based gene therapy has enjoyed great successes over the past decade, with Food and Drug Administration-approved therapeutics and a robust clinical pipeline. Nonetheless, barriers to successful translation remain. For example, advanced age is associated with impaired brain transduction, with the diminution of infectivity depending on anatomical region and capsid. Given that CNS gene transfer is often associated with neurodegenerative diseases where age is the chief risk factor, we sought to better understand the causes of this impediment. We assessed two AAV variants hypothesized to overcome factors negatively impacting transduction in the aged brain; specifically, changes in extracellular and cell-surface glycans, and intracellular transport. We evaluated a heparin sulfate proteoglycan null variant with or without mutations enhancing intracellular transport. Vectors were injected into the striatum of young adult or aged rats to address whether improving extracellular diffusion, removing glycan receptor dependence, or improving intracellular transport are important factors in transducing the aged brain. We found that, regardless of the viral capsid, there was a reduction in many of our metrics of transduction in the aged brain. However, the transport mutant was less sensitive to age, suggesting that changes in the cellular transport of AAV capsids are a key factor in age-related transduction deficiency.

INTRODUCTION

Adeno-associated virus (AAV)-mediated gene therapy for central nervous system (CNS) indications took a big step forward with the Food and Drug Administration approval of Zolgensma for the treatment of infantile spinal muscular atrophy.[1] Nonetheless, numerous gene therapy trials in the CNS, including trials for Parkinson's disease (PD), while demonstrating a strong safety profile, have failed to demonstrate efficacy in terms of disease modification.[2–4] Although the underlying reasons for this lack of translation are unclear, several hypotheses have been brought forth. For instance, there is a staunch paucity of animal models that fully recapitulate the disease etiology of sporadic forms of neurological disease, bringing into question whether gene therapy payloads will provide therapeutic translation.[5–7] Moreover, the vast majority of preclinical studies are conducted in young animals, and thus fail to account for a chief risk factor in the etiology of neurodegenerative disease, i.e., age.[8] But equally important, significant changes in transduction efficacy and transgene expression have been documented in the aged CNS depending on anatomical target and serotype. For instance, we have demonstrated that AAV 2, 5, and 9 all exhibit age-dependent reductions in transduction efficacy when delivered to the rodent basal ganglia.[9,10]

While the higher cost and availability of aged animals can be prohibitive, advanced age of experimental subjects is a critical factor for gene therapy research aimed at age-related diseases. As such, it is imperative to identify AAV capsids that do not show reduced transduction efficiency following delivery to the aged CNS. To do so, one must first identify the mechanisms conferring the apparent resistance to productive infectivity in the aged environment. Although the reason for the age-related impairment in AAV-mediated transduction remains unclear, several factors could contribute to this phenomenon. We have previously identified that specific brain regions show age-related changes in glycans, the primary receptor of AAV. Specifically, we noted an overall reduction in N-acetylated and N-sulfated heparan sulfate (HS) disaccharides (with HS proteoglycans [HSPG] being the primary receptor for AAV2) in the aged rat striatum, as well as region-specific changes in N-glycans with terminal galactose— the primary receptor for AAV9.[11] These findings suggest that the overall infectability of AAV within the aged brain declines in part as a result of altered cell receptor dynamics. Moreover, the composition of proteoglycan content changes with age and disease,[12,13] a scenario that could alter the degree to which AAV particles are sequestered extracellularly, negatively impacting diffusion and effectively reducing the multiplicity of infection (MOI).[14]

Received 22 November 2023; accepted 5 September 2024;
https://doi.org/10.1016/j.omtn.2024.102332.

Correspondence: Fredric P. Manfredsson, Parkinson's Disease Research Unit, Department of Translational Neuroscience, Barrow Neurological Institute, Phoenix, AZ 85013, USA.
E-mail: fredric.manfredsson@barrowneuro.org

Other crucial facets of AAV infection are the intracellular factors that mediate the infective cascade following receptor binding: internalization, intracellular trafficking through the endo-/lysosomal pathway, and subsequent nuclear translocation. All these cellular phenomena change with advanced cellular age. For instance, clathrin-mediated endocytosis (CME) is impaired with senescence and aging is associated with lysosomal dysregulation.[15–18] Similarly, the final transport step, nuclear translocation, is also impaired with aging.[19] All these age-related changes thus provide avenues by which AAV infectivity declines with advancing age.

AAV capsid development has exhibited a veritable explosion in the past decade with researchers utilizing various random approaches, such as directed evolution or random/guided peptide insertion, to generate large AAV libraries.[20–25] In addition, there has been a significant amount of work focused on rational design of AAV capsids, based on solved capsid structures and an improved understanding of the intracellular pathways that mediate AAV infection, and the constant identification of additional AAV receptors.[26] For instance, we and others have characterized the infectivity of various AAV trafficking phosphomimetics, carrying mutations preventing phosphorylation of key exposed surface moieties that guide the capsid to endosomal escape thus avoiding subsequent degradation.[27–29] These mutants exhibit vastly improved transduction properties when the vector is delivered to various organ systems, including following intraparenchymal injections into rodent and non-human primate brain.[27,30,31] Another engineered variant of AAV includes mutations in the binding site for the canonical receptor for AAV2: HSPG.[32] Interestingly, in contrast to early reports of strong dependence of AAV2 infection on this receptor, HSPG null mutants exhibit improved transduction properties in the CNS and in retina.[27,31,33] In addition, our previous work showed that incorporation of HSPG disrupting mutations vastly improved diffusion throughout the brain parenchyma, rivaling transduction efficacy to that seen with, for instance, AAV5 and AAV8.[27]

Following intraparenchymal delivery of AAV in human PD clinical trials (average age 57–60 years[4,34]), infectivity and diffusion were surprisingly limited in postmortem examinations.[2–4,35] We argued that one key aspect for this observed lack of translation from preclinical models to human patients is the limited AAV infectivity associated with the aged brain discussed above. Further, we hypothesized that utilizing AAV variants that can bypass such age-associated limitations, transduction efficacy, and associated therapeutic benefit would be maintained in the aged brain. Here we evaluated the infectivity and diffusion properties of two distinct AAV2 variants injected into the striatum of both young and aged rats. One variant, "HS," is an HSPG null mutant predicted to exhibit improved parenchymal diffusion and use a non-canonical receptor for entry, thus avoiding age-associated changes in HSPG receptors and extracellular matrix components. The second variant, "YH," in addition to the HS mutation, also contained tyrosine (Y) to phenylalanine (F) capsid mutations,[29] aimed at overcoming deficiencies in intracellular trafficking by improving the overall efficacy of intracellular transport. These AAV2 variants were compared for infectivity, transgene expression, diffusion, and intracellular transport relative to wild-type (WT) AAV2 in young adult (3-month-old) and aged (20-month-old) rats. Our results demonstrate that both variants, while outperforming WT AAV2, still exhibited reduced transduction efficiency with age. However, the YH variant was less impaired, especially in the context of long-range retrograde transduction, suggesting that components of intracellular transport are key mediators in conferring age-related impairments in transduction.

RESULTS

Transduction

The striatum represents a relevant clinical target for PD and is a large structure ideal for assessing vector spread. Accordingly, to evaluate the efficacy of the mutant vectors, we delivered a single 2 μL bolus of either WT or mutant AAV variants (1.0×10^{12} vg/mL) to the center of this structure in either young or aged F344 rats. To assess overall transduction, serial sections were stained for the transgene (mCherry), and the area of transgene within the confines of the striatum was outlined (Figures 1A–1F). The total numbers of transduced cells per section were enumerated using an artificial intelligence (AI) convolutional neural network (CNN) framework, and stereological principles were applied to calculate the total number of transgene+ cells per hemi-striatum (Figure 1G), which were analyzed with a two-way ANOVA (significant differences were seen for the main effects of age ($F_{(1,\ 37)} = 11.98$, $p = 0.001$), and vector ($F_{(2,37)} = 59.24$, $p < 0.0001$). Tukey honestly significant difference (HSD) post hoc tests were performed where relevant. As expected, WT AAV2 exhibited the lowest level of transduction with 17,412 and 13,088 mCherry+ cells in young and aged animals, respectively. There was not a significant difference in the number of WT AAV2 transgene+ cells between young and aged animals, similar to prior results.[10] Both mutant capsids exhibited significantly higher transduction compared with WT (HS young: 136,333 cells, HS aged: 90,467 cells, YH young: 135,051 cells; YH aged 93,841 cells; $p < 0.0005$ for all mutant capsid groups vs. young and aged animals treated with WT AAV2). Although not statistically significant, a notable decrease in the average number of transduced cells is observed with age for both mutants (HS: 33.6% decrease and YH: 30.5% decrease). Finally, because we were chiefly interested in the role of aging in transduction efficiency, we also ran an independent t test in a secondary analysis (as per Polinski et al.[10]; Figure 1H) to compare young vs. aged subjects injected in the same structure with the identical vector construct where we noted a difference with HS ($p < 0.05$) but not with YH ($p = 0.06$) or WT ($p = 0.11$).

Given that this specific AI algorithm had not previously been validated for striatal neurons, we also performed manual cell counts (stereology) of striatal sections from animals from each group. There was no difference between the number of transgene-positive cells per striatum using either methodology as assessed using a regression analysis of total number of cells ($R^2 = 0.9838$; Figure S1).

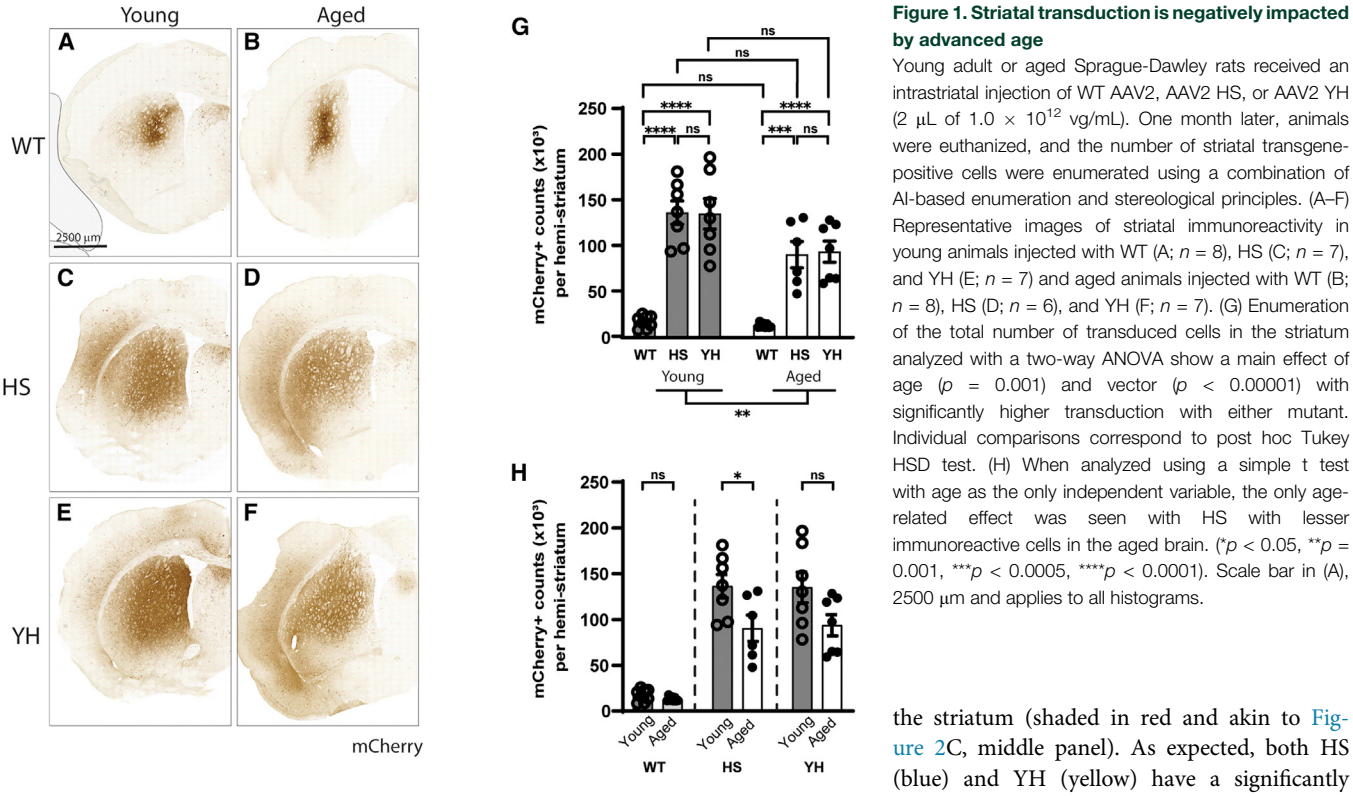

Figure 1. Striatal transduction is negatively impacted by advanced age

Young adult or aged Sprague-Dawley rats received an intrastriatal injection of WT AAV2, AAV2 HS, or AAV2 YH (2 µL of 1.0 × 10^{12} vg/mL). One month later, animals were euthanized, and the number of striatal transgene-positive cells were enumerated using a combination of AI-based enumeration and stereological principles. (A–F) Representative images of striatal immunoreactivity in young animals injected with WT (A; n = 8), HS (C; n = 7), and YH (E; n = 7) and aged animals injected with WT (B; n = 8), HS (D; n = 6), and YH (F; n = 7). (G) Enumeration of the total number of transduced cells in the striatum analyzed with a two-way ANOVA show a main effect of age (p = 0.001) and vector (p < 0.00001) with significantly higher transduction with either mutant. Individual comparisons correspond to post hoc Tukey HSD test. (H) When analyzed using a simple t test with age as the only independent variable, the only age-related effect was seen with HS with lesser immunoreactive cells in the aged brain. (*p < 0.05, **p = 0.001, ***p < 0.0005, ****p < 0.0001). Scale bar in (A), 2500 µm and applies to all histograms.

Volumetric spread

Lessons learned from clinical trials show that not only is transduction efficiency important, but so is the ability of the virus to diffuse extracellularly and infect target cells throughout a structure. This is particularly true in large areas such as the striatum, a putative target in diseases such as PD and Huntington's disease (HD). Striatal outlines in AIforia were enumerated for area and converted to volume to represent size differences in physiologically relevant terms (Figure 2A). Two-way ANOVA revealed a significant effect of vector ($F_{(2, 35)}$ = 62.93, p < 0.0001) but not age ($F_{(1, 35)}$ = 32.86, p = 0.05). Post hoc comparisons showed that WT transduced young (9.31 mm^3) and aged (7.65 mm^3) animals at a significantly smaller volume than HS (young: 22.78 mm^3, aged: 26.92 mm^3) and YH (young: 28.78 mm^3, aged: 28.94 mm^3); p < 0.0001 for all comparisons. There was no difference between transduction spread in YH compared with HS at either age, and there was no effect of age on diffusion for either vector (Figure 2B).

Additionally, to qualitatively assess the differences in the pattern of the vectors' spread with aging, we mapped the distribution of transduction within the striatum. The rat brain atlas was used as reference to create a schematic of the striatum in each plane: coronal, horizontal, and sagittal (Figure 2C) and a volumetric model (Video S1). Using the data acquired from the AIforia AI analysis of striatal tissue, we plotted: area transduced (mm^2, Figure 2D) and total mCherry+ cells (Figure 2E) per each section, along the rostro-caudal axis. Data lines are superimposed on a schematic of a dorsal view on the striatum (shaded in red and akin to Figure 2C, middle panel). As expected, both HS (blue) and YH (yellow) have a significantly higher spread than WT (orange) across the striatum measured by both area and number of transduced cells. There is no notable difference in the extent of the spread, i.e., area transduced (Figure 2D), between mutant vectors HS and YH, or with age. Similarly, when looking at the number of transduced cells, i.e., mCherry+ cell counts (Figure 2E), both mutants HS and YH display enhanced transduction when compared with WT; and no difference was observed between young and aged rats treated with WT vector. Then again, HS and YH mutants display almost identical patterns of spread in both young (dotted lines) and aged (solid lines) groups. Notably, there was a slight but nonsignificant decrease in transduction with age. Interestingly, however, an apparent shift in transduction caudally within the striatum was seen with age with all viral capsids. Finally, to facilitate visual comparison of the aforementioned results, we assigned total count of mCherry+ cells per section to a heatmap scale (Figure 2F) and overlaid this on a spatial schematic of the striatum. Figure 2G shows counts along the rostro-caudal axis on a horizontal view and the Supplemental Video shows the entire 3D reconstruction. The same data grouped by either vector or age are shown in Figure 2H.

Transgene expression

Enumerating transgene-expressing cells is rather binary and does not necessarily reflect the potency of transduction of the various AAVs since various MOIs can give rise to the same number of transgene-positive cells, but each cell may contain various degrees of transgene expression. In previous work, we showed that different capsid

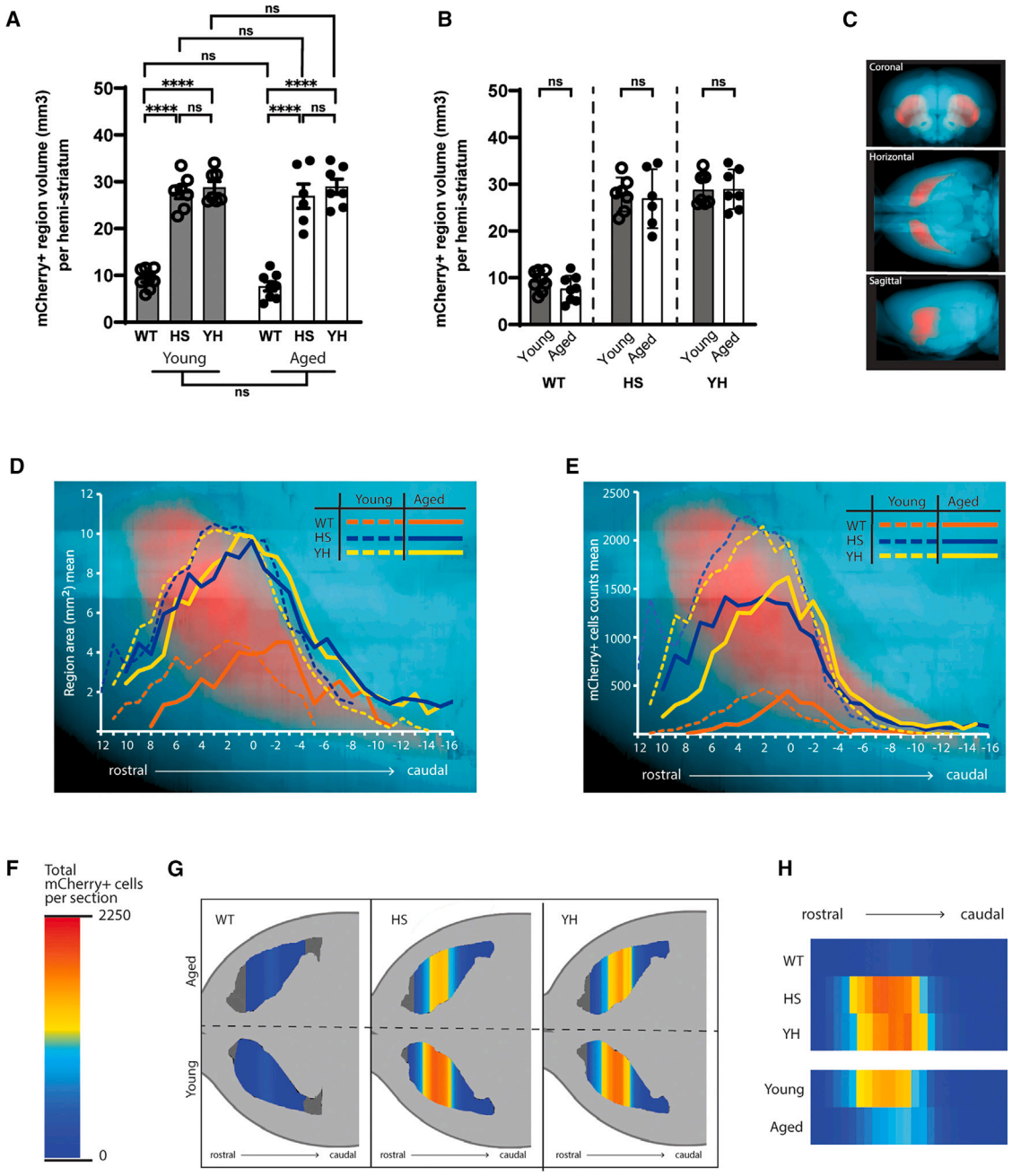

Figure 2. Volumetric distribution

In order to better understand the influence of age on striatal vector transduction we utilized the distribution of immunolabeling to outline an area of transduction and used this to calculate volume. Further we mapped transduction along the striatal rostro-caudal axis. (A) We did not observe an effect due to age, but again, both mutants transduced a much larger volume than WT. (B) No age-related effects were found when each vector was analyzed with a t test. (C) Schematic of striatum (shaded red) inside the rat brain (shaded cyan) is represented in three planes: coronal, horizontal, and sagittal. Striatum was spatially defined using reference from rat brain atlas.[36] (D) Area transduced per section and (E) mCherry+ cells per section along the rostro-caudal axis. (F–H) Transduction represented as a heatmap for visual comparison. (F) Color scale for total mCherry+ cell counts. (G) Schematic of total mCherry+ cells per section (represented by color assigned by heatmap scale on the right) overlaid across a dorsal view of the striatum. (H) transduction distribution in striatum combined per vector (top panel) or per age (bottom panel).

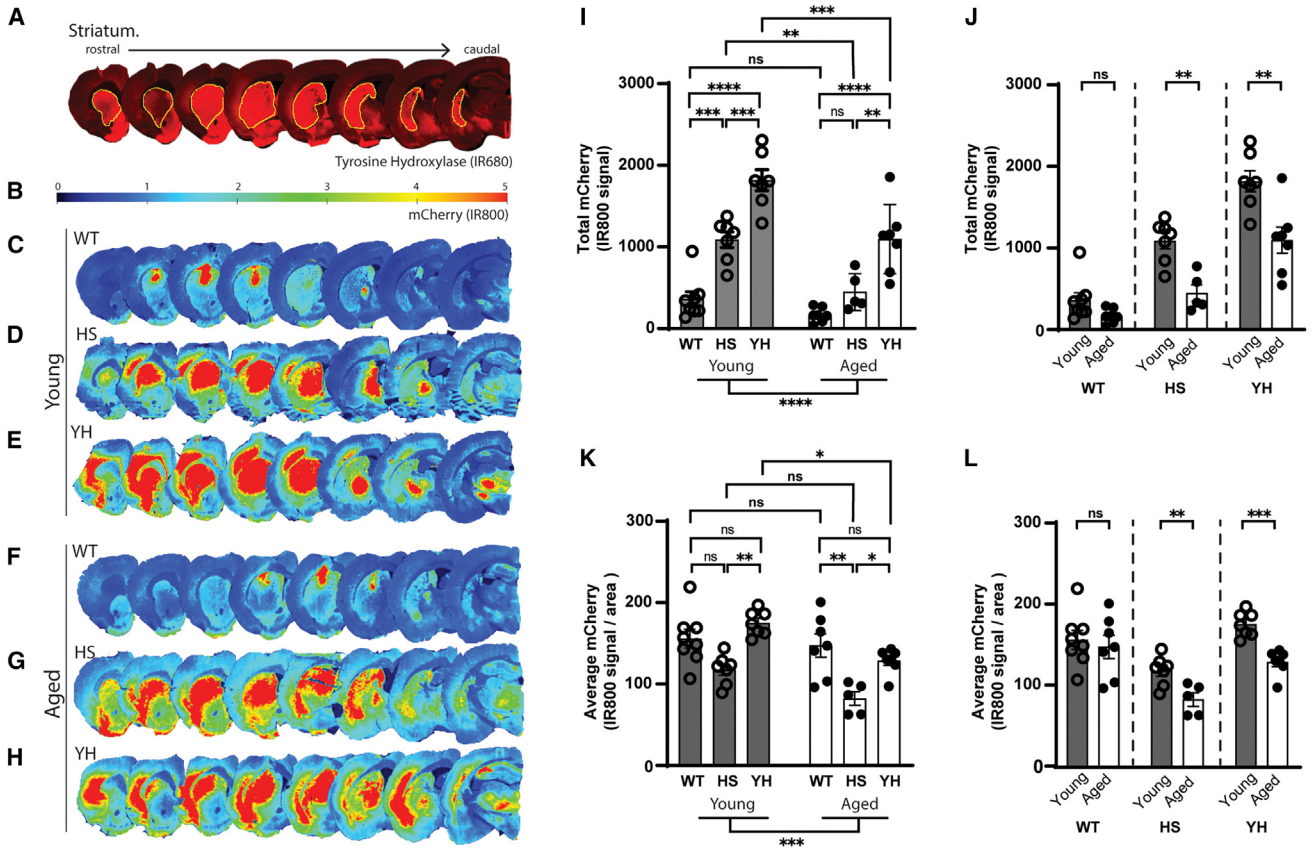

Figure 3. Striatal transgene expression is reduced with old age

Since enumeration of transgene+ cells is binary and not a full measure of infectivity, we also measured the level of transgene expression in the striatum using densitometry of near-infrared imaging. (A) To measure transgene signal, first the full striatum was outlined using TH immunoreactivity in the 680 channel, then area of mCherry+ expression was outlined using a heatmap scale in the 800 channel (B–H). Representative images of mCherry expression in young WT (C), HS (D), YH (E), and aged WT (F), HS (G), YH (H). A two-way ANOVA showed a main effect of age on both total (I) and average (signal/area; K). (J) and (L) Individual t tests showed that age negatively impacted expression in both variants but not WT. *$p < 0.05$, **$p < 0.01$, ***$p < 0.001$, ****$p < 0.0001$.

variants will exhibit a differential pattern of expression (e.g., more or less degrees of expression within a focal area).[27] Thus, given the big differences in volumetric spread of striatal transduction, we measured total and average transgene expression levels per area of striatal transduction (arbitrary units [AU]/pixel units; Figure 3). To that end, using quantitative near-infrared (nIR) imaging on the LI-COR Odyssey system, we quantified protein levels within the striatum (Figure 3) as well as total transgene expression throughout the hemisphere, including afferent and efferent areas like the substantia nigra, hippocampus, thalamus, and cortex (Figure 4).

Striatum

The striatum was first outlined (Figure 3A) based on tyrosine hydroxylase immunoreactivity, and thereafter the area of transduction was outlined within the striatum (Figures 3B–3H), thus giving us expression per area (Figures 3K and 3L) as well as total transgene levels (Figures 3I and 3J). Total expression: data normalized to non-transduced area is reported in AU (raw data divided by 10,000 for illustration purposes). A two-way ANOVA (Figure 3I) yielded a significant interaction effect between Age × Vector ($F_{(2, 35)} = 3.509$, $p < 0.05$) and a simple main effect of Age ($F_{(1, 35)} = 32.86$, $p < 0.0001$) and Vector ($F_{(2, 35)} = 62.93$, $p < 0.0001$). In contrast to previous report,[9,10] no differences in protein levels (Figures 3I and 3J) were observed between WT AAV2-treated young (Figure 3C; 361 AU) and aged (Figure 3F; 167 AU) rats. However, an age-related difference was seen with HS between young (Figure 3D; 1089 AU) and aged (Figure 3G; 448 AU) rats (Figure 3I; $p = 0.006$, as well as between YH in young (Figure 3E; 1817 AU) and aged (Figure 3H; 1097 AU) rats ($p < 0.005$; Figure 3I). Young animals treated with WT AAV showed significantly lower expression than young YH and young HS ($p < 0.0002$), while the aged WT group was only different from YH ($p < 0.0001$) but not HS. Interestingly, we observed a significant difference between HS and YH in both young and aged groups ($p = 0.0004$ and 0.006, respectively) suggesting a significant effect of the extra capsid mutation on protein expression. Again, we ran simple t tests with age as the only independent variable (Figure 3J) in which case only HS and YH show a significant decrease with age (HS [$p = 0.001$], and YH [$p = 0.004$]), but not WT ($p = 0.08$).

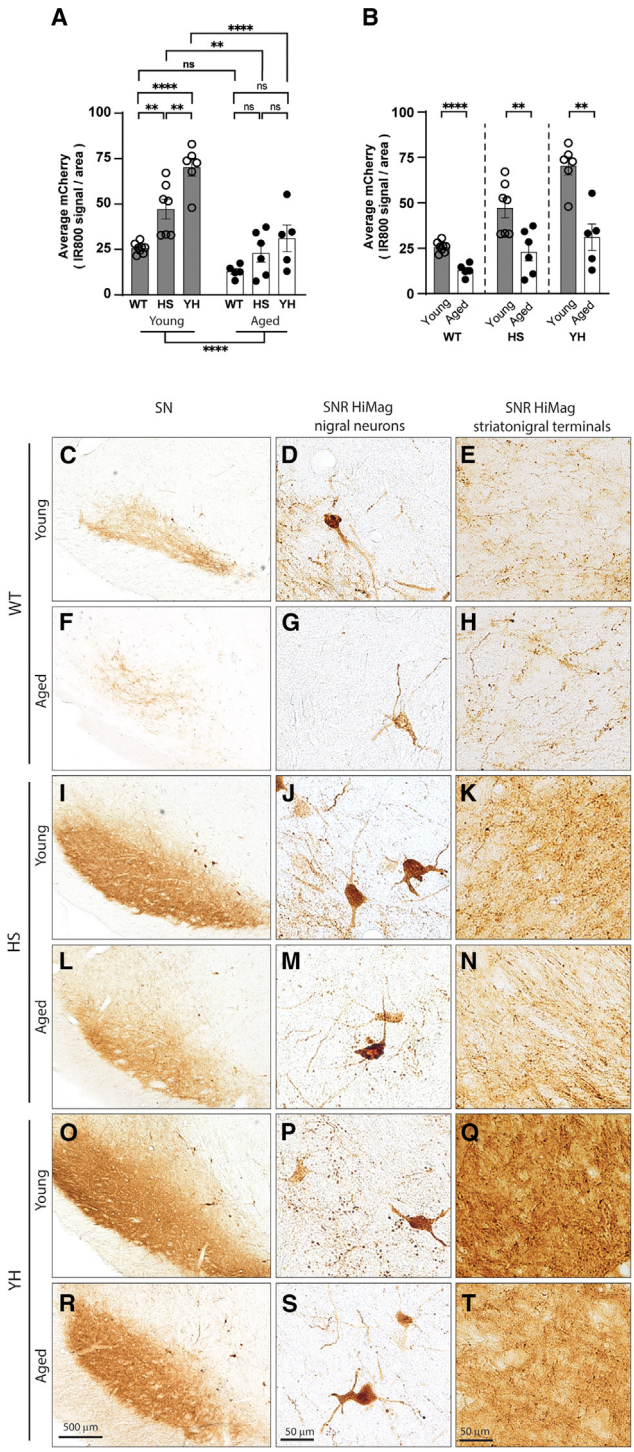

Figure 4. Transduction in the midbrain is significantly impacted by age: combination of anterograde transport of transgene to terminals and retrograde transduction of nigral cells

The midbrain region containing the SN is an important target in PD. Accordingly we quantified the total level of transgene in this area. (A) A two-way ANOVA showed a main effect of age on mCherry expression, and individual t tests (B) showed that this age-related impairment in transduction was significant across all the capsid variants. Representative images of mCherry immunoreactivity in the SN (low magnification; left panels), SNc (middle panels), and SNr (right panels) from Young WT (C–E), Aged WT (F–H), Young HS (I–K), Aged HS (L–N), Young YH (O–Q), and Aged YH (R–T). *$p < 0.05$, **$p < 0.01$, ****$p < 0.0001$. Scale bar in (R), 500 µm and applies to (C), (F), (I), (L), (O), and (R). Scale bars in (S) and (T), 50 µm and applies to (D), (E), (G), (H), (J), (K), (M), (N), (P), (Q), (S), and (T).

When we assessed the average transgene expression per area (AU; raw data divided by 100 for illustration purposes) an interesting profile emerged. Specifically, a two-way ANOVA analysis (Figure 3K) revealed a significant effect of vector ($F_{(2, 35)} = 173.1$, $p < 0.0001$) and age $F_{(1, 35)} = 141.7$, $p = 0.0006$). There was no difference between young (155.8 AU) and aged (147.3 AU) WT, or young (117.7 AU) or aged (82.32 AU) HS animals, although there was a difference in young (175.0 AU) and aged (128.7 AU) YH animals ($p < 0.05$). Interestingly, compared with the other capsids, HS provided less focal expression in younger animals than YH ($p = 0.002$), but this difference was more pronounced in aged animals ($p < 0.05$ vs. aged WT and YH), again, underscoring the additional effect of the extra capsid mutations in YH on protein expression. Individual t test analyses revealed (Figure 3L) an effect of age in HS ($p < 0.01$) and YH ($p = 0.0001$), but not WT subjects.

Substantia nigra

The midbrain area, composed of the substantia nigra (SN), pars reticulata (SNr), and the SN pars compacta (SNc), is a key target in PD, both in terms of the expression of cell-autonomous (i.e., in nigral neurons) and non–cell-autonomous factors (i.e., expression originating from striatal terminals). The entire SN was outlined and mCherry expression was measured as a function of area using LI-COR. A two-way ANOVA yielded a significant interaction effect between Age × Vector ($F_{(2, 31)} = 4.051$, $p < 0.05$) and a simple main effect of Age ($F_{(1, 31)} = 46.21$, $p < 0.0001$) and Vector ($F_{(2, 31)} = 22.79$, $p < 0.0001$). Young WT was lower in general than young HS and YH ($p < 0.01$ and $p < 0.0001$, respectively), but those differences were not significantly different in the aged animals. There was no age-related effect on expression with WT AAV2 (young-25.7, aged-12.9). However, interestingly both YH (young-70.3, aged-31.1) and HS (young-47.3, aged-23.0) exhibited a significant reduction in midbrain expression ($p < 0.01$ and <0.0001, respectively). When we analyzed expression with age as the only variable (Figure 4B), individual t test comparisons revealed significantly decreased expression in all vector groups: WT ($p < 0.0001$), HS ($p < 0.01$), and YH ($p < 0.005$). Representative images of the SN showing mCherry immunoreactivity are shown in Figures 4C–4T. Sporadic positive neuronal cell bodies were present in all groups, with most of the signal originating from striatonigral terminals.

Broad distribution

The ability to achieve robust retrograde transduction may be relevant in certain clinical settings. For example, in HD, the striatum is the chief anatomical target; however, additional anatomical structures such as the cortex and thalamus are also affected in HD.[37] The ideal gene therapy approach in such situations should

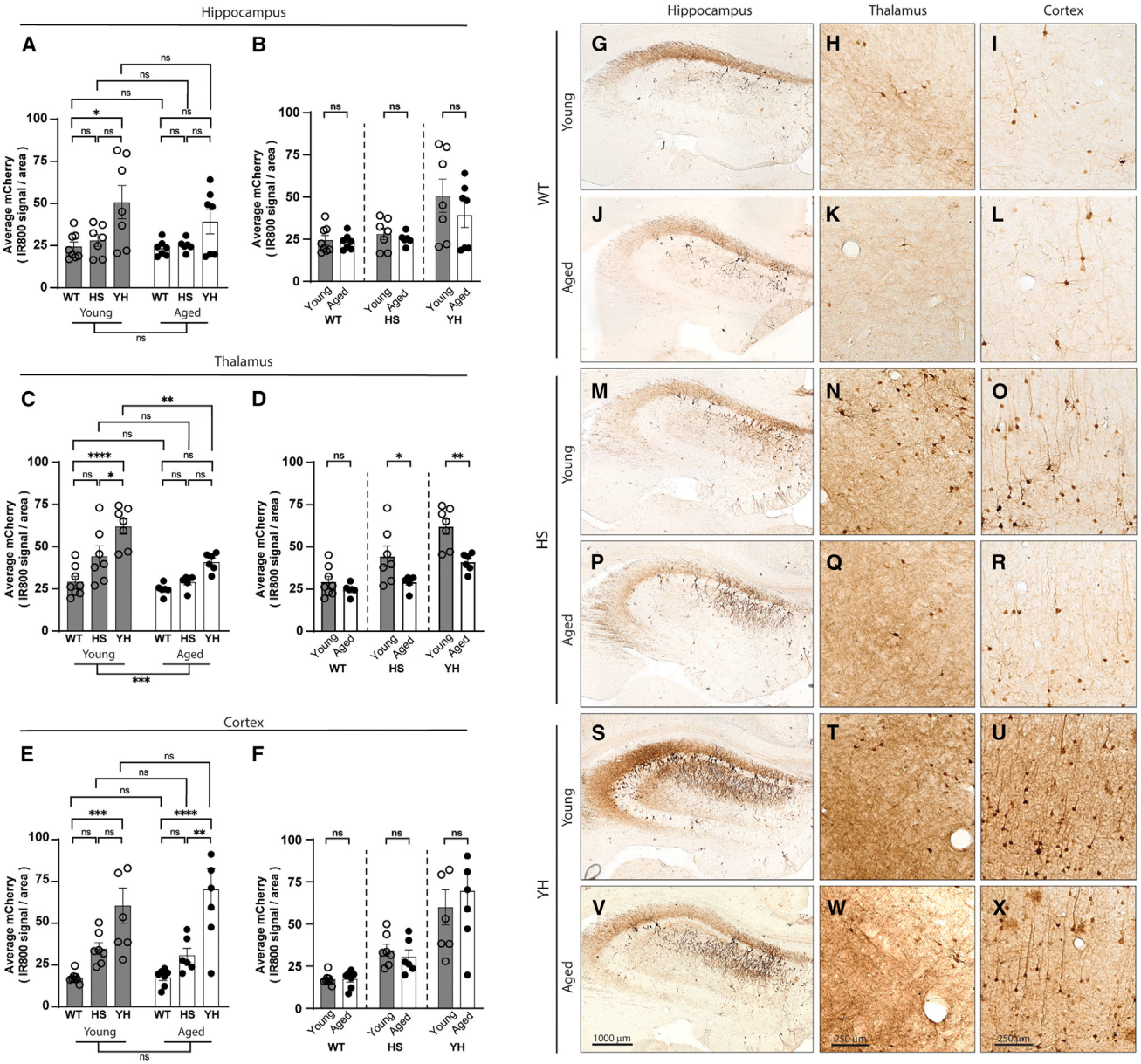

Figure 5. Retrograde transduction is significantly impacted by advanced age

Although our main anatomical target was the striatum, we also wanted to better understand the degree of infection of striatal projection areas. To that end, we outlined transduced areas of the thalamus, hippocampus (HC), and cortex (CTX) and quantified expression levels using LI-COR-assisted near-infrared densitometry. We observed a main effect of age in the thalamus (A), but not hippocampus (C) or cortex (E). Individual t tests showed a significant reduction in transgene expression in the aged thalamus across all mutant capsids (D), an effect that was not seen in the hippocampus (B) or cortex (F). Representative images of mCherry immunoreactivity in the dorsal hippocampus (left panels), medial thalamus (middle panels), and somatosensory cortex (right panels). $^{*}p < 0.05$, $^{**}p < 0.01$, $^{***}p < 0.001$, $^{****}p < 0.0001$. Scale bar in (V), 1000 μm and applies to (G), (J), (M), (P), (S), and (V). Scale bars in (W) and (X), 250 μm and applies to (H), (I), (K), (L), (N), (O), (Q), (R), (T), (U), (W), and (X).

cover multiple brain loci over a broad anatomical area. To assess retrograde transduction (Figure 5), we chose to perform LI-COR densitometric analyses of areas that would not be directly influenced by the injection sphere or needle track per se; specifically, the hippocampus and the thalamus. As previously described, the transduced area within each structure (as identified by anatomical landmarks) was outlined and transgene levels (AU) were computed as a function of area (AU raw data divided by 100 for illustration purposes).

Hippocampus: Transduction was similar between groups (young: WT- 24.4, HS- 28.0, YH- 50.7; aged: WT- 23.3, HS- 25.2, YH- 39.2)

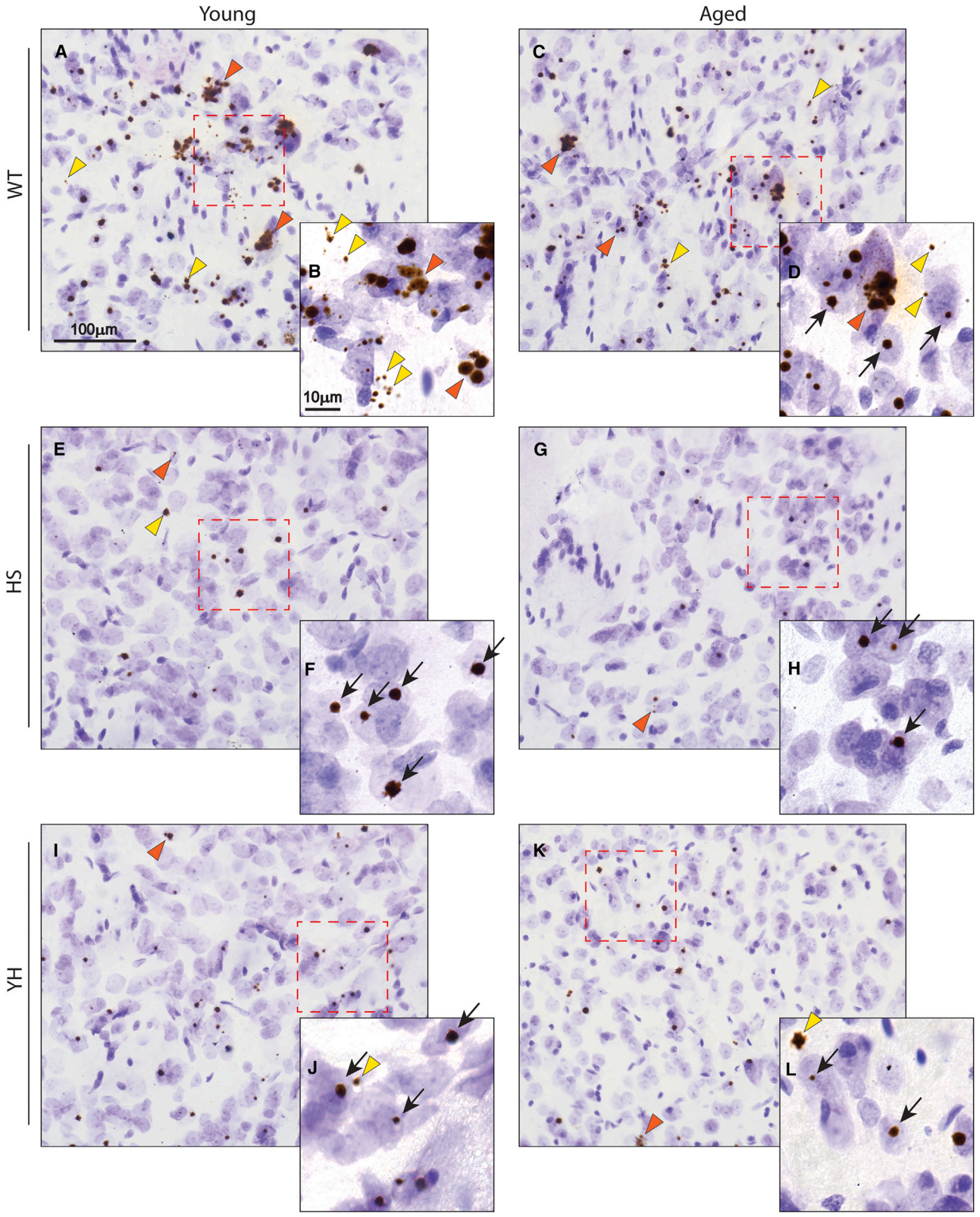

(legend on next page)

with the only significant difference emerging between young WT and YH ($p < 0.05$). It is worth noting that the average expression value for YH is much higher than the WT and HS in both age groups. However, we observed substantial variability between subjects, therefore our results failed to reach a statistically significant difference (images representing the mean are shown in Figure 5). A two-way ANOVA analysis (Figure 5A) revealed an effect of vector ($F_{(2, 36)} = 8.989$, $p = 0.0007$), but not age ($F_{(1, 36)} = 1.339$, $p = 0.25$). Individual t tests (Figure 5B) revealed no further differences due to age.

Thalamus: (Figure 5C) A two-way ANOVA yielded an effect for Vector ($F_{(2, 36)} = 21.06$, $p < 0.0001$) and Age ($F_{(1, 34)} = 19.22$, $p < 0.0001$). Young YH (61.9) exhibited significantly higher expression than young HS (44.3; $p < 0.05$) and WT (29.2; $p < 0.0001$). There was no difference between young HS and young WT, or between either aged treatment group (WT-24.7, HS-29.1, YH-40.9). There was a significant difference due to age in YH groups ($p < 0.01$). Individual t tests (Figure 5D) revealed an effect due to age with both YH and HS, but not WT.

Cortex: The cortex represents another area with significant projections to the striatum and exhibits retrograde transduction following intrastriatal injections. As described for other brain regions, cortex (as defined by outlines based on morphological landmarks), and LI-COR was used to quantify expression (Figures 5E and 5F). We observed a significant effect of Vector ($F_{(2, 36)} = 25.17$, $p < 0.0001$), but not Age ($F_{(1, 36)} = 0.1211$, $p = 0.7$; Figures 4M and 4N). Multiple comparisons revealed no differences with age (WT young-17.3, aged-17.4; HS young-34.5, aged-30.6; YH young-60.0.6, aged-69.7). YH resulted in a higher degree of cortical expression compared to young and aged WT ($p < 0.001$), and aged HS ($p < 0.01$).

Subcellular localization

To try to begin to elucidate mechanisms underlying the differences in transduction and transport, we performed RNAscope *in situ* hybridization against a non-transcribed portion of the viral genome (Figure 6). Qualitative observations revealed a diverse pattern of transduction with WT AAV2, with variable number of genomes present within the nucleus, but also with genomes persistent outside the nucleus to a higher degree than with the mutant variants. Possibly explaining the general impairment in transduction seen with the WT capsid. For both mutants (HS and YH) and age groups, the genomes are found widely distributed throughout the tissue and mostly nuclear with a single genome. Although, these data were not quantified, they are in agreement with previous reports using fluorescently tagged AAV2 capsids.[38]

Tropism

In our previous work comparing various mutants or WT AAV in young and aged animals, no overt change in vector tropism was observed. Here we qualitatively assessed the tropism of the various capsids by co-labeling transduced cells (mCherry+) with either Olig2 (oligodendrocyte transcription factor 2, oligodendrocyte marker; Figure S2), GFAP (glial fibrillary acidic protein; astrocyte marker; Figure S3), or Iba1 (Ionized calcium binding adaptor molecule 1; microglia marker; Figure S4). Transgene+ oligodendrocytes (Figure S2), were observed across capsids and age most frequently within or in proximity to the corpus callosum. Transgene+ astrocytes (Figure S3), were rare but observed in all groups in areas close to the injection site (Figures S3M–S3O). Other astrocytes that appear to display positive transduction at low magnification (Figures S3A–S3L) were found to be non-transduced, but closely associated with mCherry+ neurons upon close examination of high-magnification confocal z stacks. No transgene+ microglia were observed in either group (Figure S4). At least three striatal sections per animal and three animals per group were stained and analyzed.

DISCUSSION

The use of AAV in CNS clinical trials is becoming commonplace. However, for a variety of reasons, there has been a failure to translate preclinical findings into clinical efficacy.[5–7] One such example was the case of neurturin, which failed to demonstrate meaningful clinical improvements despite a wealth of preclinical efficacy data.[4,34] An important clue to this disconnect came from postmortem examinations of treated brains which showed significantly less AAV transduction in PD patients compared with preclinical animal studies.[2–4,35] Although there may be many reasons for this, two may be related to the fact that: (1) essentially all preclinical studies with neurturin/GDNF were done in young animals, and (2) the brain region of vector injection, involving nigrostriatal and striatonigral systems, exhibits reduced transduction efficacy with advanced age.[9,10] It is therefore clear that translational studies must consider these important variables in order to understand and predict infectivity in therapeutically relevant populations, including PD where the average age of onset is approximately 60 years of age.

In an attempt to decipher the factors that influence age-related changes in infectivity and to assess vector transduction using the clinically relevant variable of age, we utilized two AAV2-based capsid variants reflecting distinct properties as it relates to the infectious process. The first set of mutations (capsid "HS") disrupts the canonical HSPG binding receptor but exhibits a paradoxical enhancement in transduction. The second capsid variant also includes mutations

Figure 6. *In situ* hybridization of viral genomes

Striatal tissue sections for each one of the groups were processed for detection of AAV viral genomes (ISH- brown puncta) and counterstained with thionin for identification of nuclei (blue). Representative images at low and high magnification, respectively, are shown, arranged as follows: WT Young (A and B), WT Aged (C and D), HS Young (E and F), HS Aged (G and H), YH Young (I and J), YH Aged (K and L). Low-magnification images depict distribution of AAV genomes across the striatum. High-magnification images show localization of AAV genomes relative to nuclei. Black arrows indicate examples of single AAV inside a nucleus, red arrowheads indicate examples multiple genomes inside a single nucleus, and yellow arrowheads indicate examples of non-nuclear viral genomes. Scale bar in (A), 100 μm, applies to all low-magnification images (C, E, G, I, and K). Scale bar in B, 10 μm, applies to all high-magnification insets (B, D, F, H, and J).

(Y → F) preventing endosomal escape in addition to the HS mutations (capsid "YH"), thus, facilitating a higher number of virions reaching the nucleus resulting in an increased effective MOI.[28,29] To assess the effect of these mutations on overcoming age-related impairments in transduction, we compared these variants head-to-head with WT AAV2 using a variety of important parameters following a single injection into the striatum, a relevant anatomical target for several neurodegenerative and neurological disorders. Importantly, these studies were undertaken in 20-month-old rats, an age roughly analogous to a 60-year-old human,[39] the average age in PD gene therapy clinical trials.

Changes in volume and transduction

To our knowledge, this was the first study to combine AI and stereological principles to quantify transduction. Whereas AI previously has been utilized to enumerate cell populations on single histological sections,[40] in our study we were able to estimate an entire neuronal population within a defined area, deriving a physiologically relevant count for total number of transduced cells in the structure of interest in each brain hemisphere. This will become an important tool moving forward, facilitating comparisons between older studies relying upon stereology proper. Moreover, stereology is dependent on optimization of parameters at the section level and variance can be introduced dependent on subjects used for optimization, stringency of lab protocols in re-running early subjects analyzed, or definition of the profile (e.g., transgene + cell of interest) which is liable to change with familiarity and screen fatigue. In contrast, using a CNN deep learning model customized to this study and further trained on the histological images used, we were able to avoid many of the human factors that introduce variability into stereological counting while providing concrete data that future studies can use as benchmarks, or for large-scale comparisons without an added bias inherent in meta-analyses.

As was seen in prior studies, both capsid mutants exhibited significantly enhanced infectivity (Figure 1G) and volumetric (Figure 2A) spread as compared with WT AAV2 in both young and aged animals. As for previous results,[10] using the metric of infected (i.e., immunoreactive for the transgene) cells as the key readout, we did not observe a significant impact of aging on the number of infected cells (Figure 1H), nor spread (Figure 2B) with aging, with WT AAV2 or YH. Surprisingly the only difference that was seen in the number of infected cells in aged animals was a significant decrease compared with young in subjects receiving HS (Figure 1H). Interestingly, and in contrast to what we had hypothesized, when we assessed total transgene protein levels, we observed a reduction in total striatal transgene with the more infectious mutant capsids in aged animals (Figure 3J). Similarly, when normalized to area, only the mutant capsids exhibited an age-related decline in expression (Figure 3L), which again may relate to the difference in diffusion properties between WT AAV2 and tested capsid mutants, with the enhanced diffusion exhibited by the mutant effectively "drawing" infectious particles away from the center of injection. There were no quantitative differences in volumetric spread due to age (Figure 2B), and no difference in spread was seen between mutants, which both spread throughout a much larger volume than WT AAV2 (Figure 2A). An interesting qualitative observation was the apparent rostro-caudal shift in transduction with aging, which was seen with all capsids tested (Figures 2D and 2E; Video S1). While the underlying reason for this is unknown, there may be age-associated differences in structure and volume, or there may be regional differences in extracellular factors influencing diffusion and infection.

Intracellular transport of AAV is impaired with aging

Interestingly, a pattern emerged when comparing HS and YH in aged subjects. Specifically, when assessing total expression levels (Figure 3J), age had a much more profound effect on HS (58.9% decline) compared with the YH variant (39.6% decline). Since mutations affecting intracellular transport are the only differences between these capsid variants, our findings suggest that age-related changed in this cellular process is a key factor in mediating age-related effects on AAV transduction. We found further support for this idea when assessing expression in striatal projection areas requiring long-range retrograde transport of the virion such as the cortex (Figures 5E and 5F) and thalamus (Figures 5C and 5D) where the YH variant again yielded much higher transduction/transgene expression than that of HS. Although improved retrograde transport with Y → F mutations has been described in the context of the AAV-retro capsid,[41] this is the first study to establish age as an important factor in the efficacy of AAV retrograde transduction.

Finally, we assessed transgene expression in the SN, a therapeutically relevant target in the treatment of PD. Delivering trophic factors to nigral neurons via a targeted injection to the striatum can confer a therapeutic effect either in a cell non-autonomous fashion (e.g., released factors from the SNr terminals of transduced direct pathway striatal neurons) or a cell-autonomous fashion via the direct retrograde transduction of nigrostriatal dopamine neurons in the SNc. To that end, in doing our analysis, we did not segregate out terminal vs. midbrain dopamine neuron transgene expression, with our values thus accounting for both these modes of expression. With every capsid we saw a significant reduction in midbrain expression with age (Figure 4B), but again, the YH expression produced significantly higher expression. It is important to note, however, that a qualitative assessment of midbrain expression suggested that YH produced more transgene+ SNc neurons (Figures 4D–4G, 4J, 4M, 4P, and 4S) supporting the notion of enhanced retrograde transduction, but also potentially skewing the data as these cells contain high levels of transgene. This aging effect emulates what we previously observed with AAV 2, 5, and 9, all showing approximately 50% less transgene in the striatonigral system following an intrastriatal injection, suggesting a ubiquitous impairment regardless of capsid.[10] Nonetheless, the expression in the aged SN with our capsid mutants was no different from that seen in young WT brains (Figure 4A), thus, these capsid variants provide a means to overcome deficiencies seen with AAV2 in the aged brain.

Whereas this study focused on elucidating aspects of aging that can impair CNS transduction, we only evaluate a single capsid and its

derivatives. Whereas a comparative analysis with other capsids certainly is warranted, it goes beyond the scope of this work. Nevertheless, it is important to note that other naturally occurring serotypes such as AAV5, AAV8, and AAV9, and engineered variants such as AAV-retro and MNM-104, among others, exhibit strong infectivity and intracellular transport and thus represent alternative capsids for consideration.[23,42,43]

No change in tropism

We observed no changes in the overall tropism of either capsid variant. This is not unsurprising given that prior studies of AAV2 with an ablated HSPG binding motif show that the virus remains largely neurotropic.[27,31,44] Indeed, with either mutant we observed a small number of transduced astrocytes and oligodendrocytes, with no transgene-positive microglia observed.

Translational impact

It is clear from our analyses that different capsids behave differently following direct intraparenchymal delivery into the young and aged brain, and an understanding of the underlying reasons is important as one considers translational aspects of AAV CNS gene therapy. For example, a variant such as YH provides robust transduction throughout a number of structures due to retrograde infection of neurons projecting directly to the injection area, making it a strong therapeutic candidate for diseases such as HD where the transduced areas in direct contact with the injected area all exhibit dysfunction and degeneration, and represent important anatomical targets. Similarly, the significant improvement in diffusion with these mutant capsids renders them ideal when transduction of large structures, such as the striatum in PD and HD, need to be transduced. On the other hand, in this study, we chose to target the striatum as it is largely a structure encapsulated by the corpus callosum, allowing us to address biological questions such as those herein (e.g., assessing diffusion versus virion transport). However, our results highlight the large degree of diffusability when the HSPG null mutation in incorporated into the AAV2 capsid, and as was shown by Naidoo and colleagues, by simply altering the trajectory and target of injection, one can achieve close to brain-wide distribution of this vector.[31] Conversely, although WT AAV2 was much less efficient in most of our metrics, the almost complete lack of diffusion (e.g., Figure 1), provides for a vector with much greater precision, making this capsid well suited for targeted injections of small populations of neurons. Moreover, although we have not noted any overt toxicity with these mutant capsids, the changes in vector biology warrants caution, and safety of these mutants needs to be further assessed. However, one key aspect about the improved efficacy is the ability to reduce overall titer and still achieve the same effective MOI as for the WT virus. Finally, this work deals with targeted injections into the CNS, but depending on the disease, alternate routes of delivery such as intrathecal or intravenous could also be considered.

It is important to note that herein we are considering a single risk factor in disease: age. However, other risk factors may also be important considerations in gene therapy for neurological conditions. For example, sex is a risk factor in certain disorders,[45] and sex can also influence CNS transduction,[46] both in terms of infectivity and tropism. This phenomenon is, at least in part, mediated by cycling hormones[47] and their role in receptor expression and should be considered in clinical translation. Moreover, we are not assessing the efficacy of these vectors in a disease environment. For example, ongoing inflammation may have a significant impact on the behavior of AAVs, and future studies should include the assessment of these capsids in neurodegenerative disease models.

A key factor in age-related impairments is reduced intracellular transport

Herein we have taken the first step toward improving our understanding of AAV transduction efficiency incorporating a clinically meaningful variable: advancing age, where our overall goal was to better understand what biological factors underly the impairment of AAV transduction associated with aging. Although in our *a priori* hypothesis we postulated that a key aspect was the changing extracellular environment that with age would act to further sequester the "sticky" AAV2 capsid[14,48] and thus impair transduction. This seemingly was not the case since there was no difference in spread with our HS mutant with age (Figure 2B), only a reduction in transgene+ striatal neurons (Figure 1B). However, when incorporating mutations aimed at improving net intracellular trafficking to the nucleus, we did see a significant differential with aging, suggesting that intracellular transport of AAV is impaired in aged cells, either through a general reduction in transport efficacy or through increased endosomal escape. Thus, a key aspect of improving gene therapy in the aged brain is to incorporate such YF (or analogous) mutations into the AAV capsid to facilitate an increase in the effective MOI (particles making it into nucleus) and thus higher expression both locally and distally. One case when this did not hold true was when assessing expression in the SN where transgene expression was impaired in all aged groups (Figure 4B). The reason for this is likely due to impaired *anterograde* transgene transport, a common feature in aging neurons,[49] since we still observed a higher degree of retrograde transduction with the YH mutant. This agrees with our previous studies where we performed precision dissections of the SNr only and saw reduced striatonigral expression.

Conclusions

In conclusion, we show that whereas HS and YH AAV2 variants exhibit improved infectivity and diffusion over WT AAV2 in both the young and aged brain, these mutants, in some cases, also exhibit impaired efficacy in the aged brain. We observed that one key contributing factor to the reduced infectivity of AAV likely is the result of a change in the way that the virion traverses the cell in association with aging, and by reducing endosomal escape using the YH transport mutant this deficiency in effective infectivity can be partially overcome.

MATERIALS AND METHODS

Animals

Young adult (3-month-old) or aged (20-month-old) male F344 rats from the National Institutes of Aging Aged Rodent Colonies were utilized and all procedures were in accordance with the Michigan State University Institutional Animal Care and Use Committee (IACUC).

Table 1. Antibodies for immunohistochemistry

Primary antibody					Secondary antibody		
Antigen	Host/Class	Cat#	Dilution		Host/Class	Cat#	Dilution
RFP	Rabbit polyclonal	Rockland #600-401-379	IHC	1:4000	Goat anti-rabbit IgG Biotin conjugated	Millipore #AP132B	1:500
mCherry	Goat polyclonal	LS Bio # LS-C204207	IF	1:1000	Donkey anti-goat IgG Alexa Fluor®594 conjugated	Thermo-Fisher Scientific #A11058	1:500
			nIR	1:1000	Donkey anti-goat IgG IRDye®800CW conjugated	LI-COR #926-32214	1:5000
TH	Rabbit polyclonal	Millipore #AB152	nIR	1:4000	Donkey anti-rabbit IgG IRDye®680RD conjugated	LI-COR #926-68073	1:5000
Olig2	Rabbit monoclonal	Invitrogen #MA5-42372	IF	1:1000	Goat anti-rabbit Alexa Fluor®488 conjugated	Thermo-Fisher Scientific #A11008	1:500
GFAP	Mouse monoclonal	Sigma-Aldrich #G6171	IF	1:1000	Goat anti-mouse Alexa Fluor®488 conjugated	Thermo-Fisher Scientific #A11001	1:500

Rats were housed two per cage, maintained on a controlled 12-h light cycle and temperature (22°C) environment. Food and water were available *ad libitum*.

Vector production

Vectors were produced as previously described.[50] Briefly, a self-complimentary viral genome plasmid encoding mCherry under control of a truncated hybrid chicken β-actin/cytomegalovirus promoter (CBA/CAG) promoter was transfected into 293T cells together with plasmids encoding helper function (pXX6) as well as AAV rep and cap genes. Cap genes were WT AAV2, HS AAV2 (R585S, R588T, R487G), or YH AAV2 (HS mutations plus Y444F, Y500F, Y730F).[27] Cells were harvested 72 h later, and viral particles were purified using a discontinuous iodixanol gradient followed by column chromatography. Viral titers were assessed using a qPCR assay and normalized to 1.0×10^{12} vector/genomes (vg)/mL using balanced salt solution (Alcon Laboratories).

Surgery

With the lack of striatal interhemispheric connections, each hemisphere was considered an "n" of 1, and animals were randomly assigned vectors. Surgery was performed under 1.7%–2.0% isoflurane anesthesia with rats placed in a stereotaxic frame. Surgical coordinates were anterior/posterior ±0.0 medial/lateral ±3.0 mm, dorsal/ventral (from dura) −4.0 mm. The injection apparatus consisted of a Hamilton syringe fitted with a glass capillary needle coated in SigmaCote[51] (Hamilton Gas Tight syringe 80,000, 26 s/2″ needle [Hamilton]). The capillary was lowered to the injection site and 2 μL vector was injected at a rate of 0.5 μL/min. Following vector delivery, the needle remained in place for 1 min, after which it was raised 1 mm and held in placed for an additional 4 min before being fully retracted.

Euthanasia

Four weeks following the vector delivery, animals were euthanized in accordance with the recommendations of the American Veterinary Medical Association and as approved by the Michigan State University IACUC. Rats were deeply anesthetized with an intraperitoneal injection of 60 mg/kg pentobarbital then transcardially perfused with Tyrode's solution followed by ice-cold 4% paraformaldehyde. Brains were thereafter placed in 4% paraformaldehyde for 24 h after which they were placed in 30% sucrose (in 0.1M PO4). Once dehydrated in sucrose, brains were cut coronally into 40-μm-thick sections using a freezing stage sliding microtome. Sections for each brain were serially distributed into six groups, arranged in plates filled with cryoprotectant, and stored in −20°C until used.

Immunostaining of brain sections

All immunostaining procedures (i.e., immunohistochemistry [IHC], immunofluorescence [IF], and LI-COR near-infrared [nIR] imaging) were performed on free-floating sections as previously described.[52] Sections for brightfield imaging were quenched with 0.3% hydrogen peroxide, followed by blocking in the appropriate serum. Sections were incubated in primary antibody overnight at room temperature (RT), and thereafter in the appropriate secondary antibodies for 2 h at RT. Brightfield sections (treated with biotinylated secondary antibodies) were incubated with an avidin-biotin complex as per manufacturer instructions (Vector ABC kit) to amplify signal and thereafter developed using 3,3′ diaminobenzidine and 0.03% hydrogen peroxide in tris buffer. IF or nIR sections were immediately mounted following incubation with secondary antibody. Sections were mounted on subbed slides, dehydrated using increasing concentrations of ethanol followed by xylene, and coverslipped using Cytoseal (Fisher Scientific) for IHC and DPX (Sigma Cat# 06522) for IF and nIR. Antibody details are listed in Table 1.

RNAscope *in situ* hybridization of AAV genomes

In order to assess subcellular localization of vector genomes, we performed *in situ* hybridization (ISH) using a probe against a non-transcribed portion of the genome paired with a Nissl (thionin) stain. ISH was carried out using the Advanced Cell Diagnostic RNAscope2.5 HD detection Kit-Brown (ACD, Cat#322310) and probe CMV-Enh-CBA promoter-O4-C1 (ACD, Cat#1211301-C1). Protocol was carried out as suggested by the manufacturer's instructions with a few modifications for 40-μM free-floating frozen

sections.[53] First, the sections were washed with TBS 6 × 5 min to remove cryoprotectant. Sections were then incubated with peroxide treatment for 45 min at RT, washed 3 × 5 min. Sections were mounted onto Superfrost Plus+ slides and air-dried for approximately 20 min, then washed three times in H_2O to remove salts and air-dried overnight at RT. The following day, sections were incubated in target retrieval solution pre-heated to 99°C–100°C for 10 min followed immediately by four times wash in H_2O, then eight times in 100% ethanol and allowed to air-dry before drawing a hydrophobic barrier. Next, protease (protease III) treatment, probe hybridization, signal amplification, and signal detection steps were carried out exactly as described per the manufacturer's protocol. After the final rinse, sections were allowed to air-dry overnight at RT. The following day, sections were counterstained with thionin. Briefly, slides were rehydrated in H_2O for 2 min, stained with thionin working solution for 8 min, rinsed twice in H_2O for 2 min each, then serially dehydrated in ethanol (70%, 95%, 100%, 1 min each), cleared in xylene for 2 min and coverslipped using Cytoseal mounting media.

Imaging

Slides for AI-based quantitation of mCherry+ cells were imaged on a ZEISS Axioscan (ZEISS Group; Oberkochen, Germany). Each scan consisted of a series of image tiles acquired across the X-Y plane, in the tissue area with positive mCherry signal. In addition, each tile consisted of a stack of images acquired with the ×20 objective across 13 μm on the z axis with a 0.8-μm step size. Finally, acquired photomicrographs were processed and stitched together by the ZEN advanced software, producing a single high-resolution digital image per each scan. Other brightfield images were acquired on a Nikon Eclipse Ni microscope. Sections stained with LI-COR secondary nIR antibodies were scanned on the LI-COR Odyssey CLx at 21 μm resolution for SN and 84 μm resolution for the rest of the brain regions. Fluorescent images were taken on a Nikon A1R HD25 confocal imaging system using a ×60 objective, z stacks were acquired at 0.2 μm steps across the thickness of the section. Representative images were selected from subjects that displayed mean values in terms of transduced cells or transgene expression.

AI-based enumeration of transduced cells and volumetric and stereological conversion

Although we observed transduction in areas beyond the striatum, we focused quantitation on the striatum. Sections were uploaded to an image analysis platform developed by AIforia (AIforia Technologies, Helsinki, Finland), which uses individualized AI deep CNN learning to facilitate quantitative histological image analysis.[40] Briefly, high-resolution brightfield photomicrographs acquired using the ZEISS Axioscan were imported into AIforia software. Striatal regions of interest, limited to the areas of transduction and guided using a rat brain atlas,[36] were outlined using a contour tool in AIforia. A custom-developed deep learning process was used to train a CNN to enumerate the total number of transduced cells and to calculate the region area of transduction. After automated counting, stereological mathematical principles were applied to derive a per-hemisphere total count of vector-positive neurons and transduction spread (region area). To derive transduced cell counts, the final number from automation was summed across sections and multiplied by the reciprocal of serial section interval (×6) (Equation 1).

Equation 1. Calculation for stereological estimation of cell numbers based on AI enumeration

$$C_H = \sum_{i_s=1}^{n_s} c_{v+} \times \left(\frac{1}{6}\right)^{-1} \quad \text{(Equation 1)}$$

where C_H is the total counts (C) for a hemisphere (H), derived by suμing (Σ) the vector-positive profile counts (c_{v+}) for each section (s) ranging from one section (i_s) to the total number of sections (n_s), then multiplying the sum by the reciprocal of the section interval (constant of 1/6).

Inherent in this workflow is the stereological principle through the preservation of systematic random sampling while further subsampling within each section. Thus, subsampling one in six sections as would be accomplished using a stereology program is obviated by use of the AI software. Total region volume was determined by summing the immunolabeled spread within the contour to derive a total transduction area for the section series. As with neuron counts, this number was multiplied by the reciprocal of serial section interval (×6) and then by the section cut thickness (×0.04 mm) (Equation 2).

Equation 2. Calculation for volumetric estimation of transduction

$$V_H = \sum_{i_s=1}^{n_s} a_{v+} \times \left(\frac{1}{6}\right)^{-1} \times 0.04 \quad \text{(Equation 2)}$$

where V_H is the total regional volume (V) for a hemisphere (H), derived by summing (Σ) the vector-positive regional area (a_{v+}) for eaμch section (s) ranging from one section (i_s) to the total number of sections (n_s), then multiplying the sum by the reciprocal of the section interval (constant of 1/6) and by the volume of section thickness (constant of 0.04 mm).

The methodology was also validated using traditional stereology per our established methodology.[54] Immunostained tissue sections from one to two animals/group (seven in total) was utilized. The region of interest was outlined at a low magnification (4×) based on the area containing RFP+ cells throughout the rostro-caudal extent of the striatum. The Paxinos and Watson rat brain atlas was used a reference to precisely identify the borders of this region.[36] Every sixth section was sampled using the optical fractionator method with a counting frame size of 175 × 175 μm and a grid size of 600 × 600 μm in Stereo Investigator software (Version 2020 1.1; Microbrightfield, Inc., Williston, VT, USA). Counting of cells was performed using a ×40 objective on a Nikon Eclipse Ni-E microscope equipped with a motorized XY stage (Ludl Electronic Products, Hawthorne, NY, USA). The coefficient of error for each estimate was calculated and found to be less than 0.1 (Gundersen, m = 1). The results for each striatum (stereology or AI enumeration) were assessed using a regression analysis (Figure S1). An aid to conversion from AI enumeration

to total population estimates and volume has been established at https://cmkdataneuro.com/stereology (please cite the current manuscript).

LI-COR-based quantitation of transgene expression

Due to the broad dynamic range, the use of near-infrared imaging provides a robust alternative to biochemical methods (e.g., PCR) to quantify transduction in fixed tissue. First, brain anatomical regions of interest were outlined in the IR680 channel defined by morphological landmarks for hippocampus, cortex, and thalamus, and by the presence of TH immunoreactivity in the striatum and SN. Following, the IR800 channel (i.e., mCherry expression) was displayed as a heatmap (Figures 3C–3H) and regions of interest were drawn around mCherry+ signal defined as >3 AU in the heatmap scale (Figure 3B). A total of 15 sections were included for analysis of the striatum, seven sections for hippocampus, thalamus, and cortex, and eight sections for the SN.

Statistics

Power analyses were performed to determine required sample sizes to detect a statistical difference at $p < 0.05$ with a power of 0.8. Our only exclusion criterion (complete absence of transduction) was established *a priori*. All data were collected by experimenters blinded to the experimental conditions. Two-way analysis of variance (ANOVA) tests were used to detect statistical significance between all groups with age (young, aged) and vector capsid (WT, HS, YH) as the independent variables. To further define any relationship across, within, and between variables, Tukey HSD post hoc test was used where a main or interaction factor significance was found. To compare young adult vs. aged rats injected in the same structure with the identical vector construct, independent t tests were used to assess the effect of age on each capsid.[10] For all analyses, a p value of less than or equal to 0.05 was considered statistically significant. All statistics were conducted in Prism (GraphPad) or R (4.1.0, build "Camp Pontanezen") using base libraries.

DATA AND CODE AVAILABILITY

The data necessary to interpret, verify, and extend the findings of this study will be available upon request.

ACKNOWLEDGMENTS

We would like to thank Nathan Kuhn and Angela Velazquez for technical assistance. This work was supported by Barrow Neurological Foundation, NIH R56 AG052328-01 (F.P.M.).

AUTHOR CONTRIBUTIONS

F.P.M., I.M.S.: Conceived the project, designed experiments, performed data analysis, and wrote the first draft of the manuscript. C.M.K.: Wrote the code for the processing of histological data and assisted with data analysis. S.E.B., S.L.B., S.M.C.: Assisted with mutant design and vector production. K.S.-C., D.J.M., M.D., L.D.B.-C., S.M.C.: Assisted with the execution of the study. All authors critically read the manuscript.

DECLARATION OF INTERESTS

I.M.S.: Co-founder of *n*Vector. Has received financial support from Aspen Neurosciences. F.P.M.: Co-founder of *n*Vector Therapeutics, CavGene Therapeutics, and Neuralina Therapeutics. Has received financial support from Regenex Bio, Aspen Neurosciences, Seelos Therapeutics. K.S.-C.: Co-founder of CavGene Therapeutics, Inc, which holds intellectual property in CaV1.3 gene silencing and has received financial support from Regenex Bio. S.E.B.: Co-founder of Atsena Therapeutics. S.L.B.: Co-founder of Atsena Therapeutics. M.D.: Co-founder of rAAVEN. D.J.M.: Has received financial support from FujiFilm Cellular Dynamics Inc and Aspen Neurosciences. Currently an employee of Biogen. I.M.S., F.P.M., S.E.B., S.L.B., and M.D. hold patents related to AAV technology.

SUPPLEMENTAL INFORMATION

Supplemental information can be found online at https://doi.org/10.1016/j.omtn.2024.102332.

REFERENCES

1. Al-Zaidy, S., Pickard, A.S., Kotha, K., Alfano, L.N., Lowes, L., Paul, G., Church, K., Lehman, K., Sproule, D.M., Dabbous, O., et al. (2019). Health outcomes in spinal muscular atrophy type 1 following AVXS-101 gene replacement therapy. Pediatr. Pulmonol. *54*, 179–185. https://doi.org/10.1002/ppul.24203.

2. Bartus, R.T., Herzog, C.D., Chu, Y., Wilson, A., Brown, L., Siffert, J., Johnson, E.M., Jr., Olanow, C.W., Mufson, E.J., and Kordower, J.H. (2011). Bioactivity of AAV2-neurturin gene therapy (CERE-120): differences between Parkinson's disease and nonhuman primate brains. Mov. Disord. *26*, 27–36. https://doi.org/10.1002/mds.23442.

3. Chu, Y., Bartus, R.T., Manfredsson, F.P., Olanow, C.W., and Kordower, J.H. (2020). Long-term post-mortem studies following neurturin gene therapy in patients with advanced Parkinson's disease. Brain *143*, 960–975. https://doi.org/10.1093/brain/awaa020.

4. Marks, W.J., Jr., Bartus, R.T., Siffert, J., Davis, C.S., Lozano, A., Boulis, N., Vitek, J., Stacy, M., Turner, D., Verhagen, L., et al. (2010). Gene delivery of AAV2-neurturin for Parkinson's disease: a double-blind, randomised, controlled trial. Lancet Neurol. *9*, 1164–1172. https://doi.org/10.1016/S1474-4422(10)70254-4.

5. Fischer, D.L., Gombash, S.E., Kemp, C.J., Manfredsson, F.P., Polinski, N.K., Duffy, M.F., and Sortwell, C.E. (2016). Viral Vector-Based Modeling of Neurodegenerative Disorders: Parkinson's Disease. Methods Mol. Biol. *1382*, 367–382. https://doi.org/10.1007/978-1-4939-3271-9_26.

6. Manfredsson, F.P., Polinski, N.K., Subramanian, T., Boulis, N., Wakeman, D.R., and Mandel, R.J. (2020). The Future of GDNF in Parkinson's Disease. Front. Aging Neurosci. *12*, 593572. https://doi.org/10.3389/fnagi.2020.593572.

7. Manfredsson, F.P., Bloom, D.C., and Mandel, R.J. (2012). Regulated protein expression for *in vivo* gene therapy for neurological disorders: progress, strategies, and issues. Neurobiol. Dis. *48*, 212–221. https://doi.org/10.1016/j.nbd.2012.03.001.

8. Collier, T.J., Kanaan, N.M., and Kordower, J.H. (2011). Ageing as a primary risk factor for Parkinson's disease: evidence from studies of non-human primates. Nat. Rev. Neurosci. *12*, 359–366. https://doi.org/10.1038/nrn3039.

9. Polinski, N.K., Gombash, S.E., Manfredsson, F.P., Lipton, J.W., Kemp, C.J., Cole-Strauss, A., Kanaan, N.M., Steece-Collier, K., Kuhn, N.C., Wohlgenant, S.L., and Sortwell, C.E. (2015). Recombinant adenoassociated virus 2/5-mediated gene transfer is reduced in the aged rat midbrain. Neurobiol. Aging *36*, 1110–1120. https://doi.org/10.1016/j.neurobiolaging.2014.07.047.

10. Polinski, N.K., Manfredsson, F.P., Benskey, M.J., Fischer, D.L., Kemp, C.J., Steece-Collier, K., Sandoval, I.M., Paumier, K.L., and Sortwell, C.E. (2016). Impact of age and vector construct on striatal and nigral transgene expression. Mol. Ther. Methods Clin. Dev. *3*, 16082. https://doi.org/10.1038/mtm.2016.82.

11. Raghunathan, R., Polinski, N.K., Klein, J.A., Hogan, J.D., Shao, C., Khatri, K., Leon, D., McComb, M.E., Manfredsson, F.P., Sortwell, C.E., and Zaia, J. (2018). Glycomic and Proteomic Changes in Aging Brain Nigrostriatal Pathway. Mol. Cell. Proteomics *17*, 1778–1787. https://doi.org/10.1074/mcp.RA118.000680.

12. van Horssen, J., Wesseling, P., van den Heuvel, L.P.W.J., de Waal, R.M.W., and Verbeek, M.M. (2003). Heparan sulphate proteoglycans in Alzheimer's disease and amyloid-related disorders. Lancet Neurol. *2*, 482–492. https://doi.org/10.1016/s1474-4422(03)00484-8.

13. Jenkins, H.G., and Bachelard, H.S. (1988). Developmental and age-related changes in rat brain glycosaminoglycans. J. Neurochem. *51*, 1634–1640. https://doi.org/10.1111/j.1471-4159.1988.tb01134.x.

14. Perabo, L., Goldnau, D., White, K., Endell, J., Boucas, J., Humme, S., Work, L.M., Janicki, H., Hallek, M., Baker, A.H., and Büning, H. (2006). Heparan sulfate proteoglycan binding properties of adeno-associated virus retargeting mutants and consequences for their *in vivo* tropism. J. Virol. *80*, 7265–7269. https://doi.org/10.1128/JVI.00076-06.

15. Lopez-Otin, C., Blasco, M.A., Partridge, L., Serrano, M., and Kroemer, G. (2023). Hallmarks of aging: An expanding universe. Cell *186*, 243–278. https://doi.org/10.1016/j.cell.2022.11.001.

16. Burrinha, T., Cunha, C., Hall, M.J., Lopes-da-Silva, M., Seabra, M.C., and Guimas Almeida, C. (2023). Deacidification of endolysosomes by neuronal aging drives synapse loss. Traffic *24*, 334–354. https://doi.org/10.1111/tra.12889.

17. Nixon, R.A. (2020). The aging lysosome: An essential catalyst for late-onset neurodegenerative diseases. Biochim. Biophys. Acta. Proteins Proteom. *1868*, 140443. https://doi.org/10.1016/j.bbapap.2020.140443.

18. Shin, E.Y., Soung, N.K., Schwartz, M.A., and Kim, E.G. (2021). Altered endocytosis in cellular senescence. Ageing Res. Rev. *68*, 101332. https://doi.org/10.1016/j.arr.2021.101332.

19. Martins, F., Sousa, J., Pereira, C.D., da Cruz E Silva, O.A.B., and Rebelo, S. (2020). Nuclear envelope dysfunction and its contribution to the aging process. Aging Cell *19*, e13143. https://doi.org/10.1111/acel.13143.

20. Koerber, J.T., Jang, J.H., and Schaffer, D.V. (2008). DNA shuffling of adeno-associated virus yields functionally diverse viral progeny. Mol. Ther. *16*, 1703–1709. https://doi.org/10.1038/mt.2008.167.

21. Koerber, J.T., Maheshri, N., Kaspar, B.K., and Schaffer, D.V. (2006). Construction of diverse adeno-associated viral libraries for directed evolution of enhanced gene delivery vehicles. Nat. Protoc. *1*, 701–706. https://doi.org/10.1038/nprot.2006.93.

22. Maheshri, N., Koerber, J.T., Kaspar, B.K., and Schaffer, D.V. (2006). Directed evolution of adeno-associated virus yields enhanced gene delivery vectors. Nat. Biotechnol. *24*, 198–204. https://doi.org/10.1038/nbt1182.

23. Davidsson, M., Wang, G., Aldrin-Kirk, P., Cardoso, T., Nolbrant, S., Hartnor, M., Mudannayake, J., Parmar, M., and Björklund, T. (2019). A systematic capsid evolution approach performed *in vivo* for the design of AAV vectors with tailored properties and tropism. Proc. Natl. Acad. Sci. USA *116*, 27053–27062. https://doi.org/10.1073/pnas.1910061116.

24. Borner, K., Kienle, E., Huang, L.Y., Weinmann, J., Sacher, A., Bayer, P., Stullein, C., Fakhiri, J., Zimmermann, L., Westhaus, A., et al. (2020). Pre-arrayed Pan-AAV Peptide Display Libraries for Rapid Single-Round Screening. Mol. Ther. *28*, 1016–1032. https://doi.org/10.1016/j.ymthe.2020.02.009.

25. Kellish, P.C., Marsic, D., Crosson, S.M., Choudhury, S., Scalabrino, M.L., Strang, C.E., Hill, J., McCullough, K.T., Peterson, J.J., Fajardo, D., et al. (2023). Intravitreal injection of a rationally designed AAV capsid library in non-human primate identifies variants with enhanced retinal transduction and neutralizing antibody evasion. Mol. Ther. *31*, 3441–3456. https://doi.org/10.1016/j.ymthe.2023.10.001.

26. Meyer, N.L., and Chapman, M.S. (2022). Adeno-associated virus (AAV) cell entry: structural insights. Trends Microbiol. *30*, 432–451. https://doi.org/10.1016/j.tim.2021.09.005.

27. Kanaan, N.M., Sellnow, R.C., Boye, S.L., Coberly, B., Bennett, A., Agbandje-McKenna, M., Sortwell, C.E., Hauswirth, W.W., Boye, S.E., and Manfredsson, F.P. (2017). Rationally Engineered AAV Capsids Improve Transduction and Volumetric Spread in the CNS. Mol. Ther. Nucleic Acids *8*, 184–197. https://doi.org/10.1016/j.omtn.2017.06.011.

28. Zhong, L., Li, B., Jayandharan, G., Mah, C.S., Govindasamy, L., Agbandje-McKenna, M., Herzog, R.W., Weigel-Van Aken, K.A., Hobbs, J.A., Zolotukhin, S., et al. (2008). Tyrosine-phosphorylation of AAV2 vectors and its consequences on viral intracellular trafficking and transgene expression. Virology *381*, 194–202. https://doi.org/10.1016/j.virol.2008.08.027.

29. Zhong, L., Li, B., Mah, C.S., Govindasamy, L., Agbandje-McKenna, M., Cooper, M., Herzog, R.W., Zolotukhin, I., Warrington, K.H., Jr., Weigel-Van Aken, K.A., et al. (2008). Next generation of adeno-associated virus 2 vectors: point mutations in tyrosines lead to high-efficiency transduction at lower doses. Proc. Natl. Acad. Sci. USA *105*, 7827–7832. https://doi.org/10.1073/pnas.0802866105.

30. Boye, S.L., Bennett, A., Scalabrino, M.L., McCullough, K.T., Van Vliet, K., Choudhury, S., Ruan, Q., Peterson, J., Agbandje-McKenna, M., and Boye, S.E. (2016). Impact of Heparan Sulfate Binding on Transduction of Retina by Recombinant Adeno-Associated Virus Vectors. J. Virol. *90*, 4215–4231. https://doi.org/10.1128/JVI.00200-16.

31. Naidoo, J., Stanek, L.M., Ohno, K., Trewman, S., Samaranch, L., Hadaczek, P., O'Riordan, C., Sullivan, J., San Sebastian, W., Bringas, J.R., et al. (2018). Extensive Transduction and Enhanced Spread of a Modified AAV2 Capsid in the Non-human Primate CNS. Mol. Ther. *26*, 2418–2430. https://doi.org/10.1016/j.ymthe.2018.07.008.

32. Summerford, C., and Samulski, R.J. (1998). Membrane-associated heparan sulfate proteoglycan is a receptor for adeno-associated virus type 2 virions. J. Virol. *72*, 1438–1445.

33. Crosson, S.M., Bennett, A., Fajardo, D., Peterson, J.J., Zhang, H., Li, W., Leahy, M.T., Jennings, C.K., Boyd, R.F., Boye, S.L., et al. (2021). Effects of Altering HSPG Binding and Capsid Hydrophilicity on Retinal Transduction by AAV. J. Virol. *95*, e02440-20. https://doi.org/10.1128/JVI.02440-20.

34. Warren Olanow, C., Bartus, R.T., Baumann, T.L., Factor, S., Boulis, N., Stacy, M., Turner, D.A., Marks, W., Larson, P., Starr, P.A., et al. (2015). Gene delivery of neurturin to putamen and substantia nigra in Parkinson disease: A double-blind, randomized, controlled trial. Ann. Neurol. *78*, 248–257. https://doi.org/10.1002/ana.24436.

35. Chu, Y., and Kordower, J.H. (2023). Post-Mortem Studies of Neurturin Gene Therapy for Parkinson's Disease: Two Subjects with 10 Years CERE120 Delivery. Mov. Disord. *38*, 1728–1736. https://doi.org/10.1002/mds.29518.

36. Paxinos, G., and Watson, C. (2006). The Rat Brain in Stereotaxic Coordinates: Hard Cover Edition (Elsevier).

37. Raymond, L.A., André, V.M., Cepeda, C., Gladding, C.M., Milnerwood, A.J., and Levine, M.S. (2011). Pathophysiology of Huntington's disease: time-dependent alterations in synaptic and receptor function. Neuroscience *198*, 252–273. https://doi.org/10.1016/j.neuroscience.2011.08.052.

38. Lux, K., Goerlitz, N., Schlemminger, S., Perabo, L., Goldnau, D., Endell, J., Leike, K., Kofler, D.M., Finke, S., Hallek, M., and Büning, H. (2005). Green fluorescent protein-tagged adeno-associated virus particles allow the study of cytosolic and nuclear trafficking. J. Virol. *79*, 11776–11787. https://doi.org/10.1128/JVI.79.18.11776-11787.2005.

39. Sengupta, P. (2013). The Laboratory Rat: Relating Its Age With Human's. Int. J. Prev. Med. *4*, 624–630.

40. Penttinen, A.M., Parkkinen, I., Blom, S., Kopra, J., Andressoo, J.O., Pitkänen, K., Voutilainen, M.H., Saarma, M., and Airavaara, M. (2018). Implementation of deep neural networks to count dopamine neurons in substantia nigra. Eur. J. Neurosci. *48*, 2354–2361. https://doi.org/10.1111/ejn.14129.

41. Nakahama, R., Saito, A., Nobe, S., Togashi, K., Suzuki, I.K., Uematsu, A., and Emoto, K. (2022). The tyrosine capsid mutations on retrograde adeno-associated virus accelerates gene transduction efficiency. Mol. Brain *15*, 70. https://doi.org/10.1186/s13041-022-00957-0.

42. Surdyka, M.M., and Figiel, M. (2021). Retrograde capabilities of adeno-associated virus vectors in the central nervous system. Biotechnologia *102*, 473–478. https://doi.org/10.5114/bta.2021.111111.

43. Tervo, D.G.R., Hwang, B.Y., Viswanathan, S., Gaj, T., Lavzin, M., Ritola, K.D., Lindo, S., Michael, S., Kuleshova, E., Ojala, D., et al. (2016). A Designer AAV Variant Permits Efficient Retrograde Access to Projection Neurons. Neuron *92*, 372–382. https://doi.org/10.1016/j.neuron.2016.09.021.

44. Sullivan, J.A., Stanek, L.M., Lukason, M.J., Bu, J., Osmond, S.R., Barry, E.A., O'Riordan, C.R., Shihabuddin, L.S., Cheng, S.H., and Scaria, A. (2018). Rationally designed AAV2 and AAVrh8R capsids provide improved transduction in the retina and brain. Gene Ther. *25*, 205–219. https://doi.org/10.1038/s41434-018-0017-8.

45. Bianco, A., Antonacci, Y., and Liguori, M. (2023). Sex and Gender Differences in Neurodegenerative Diseases: Challenges for Therapeutic Opportunities. Int. J. Mol. Sci. *24*, 6354. https://doi.org/10.3390/ijms24076354.

46. Maguire, C.A., Crommentuijn, M.H., Mu, D., Hudry, E., Serrano-Pozo, A., Hyman, B.T., and Tannous, B.A. (2013). Mouse gender influences brain transduction by intravascularly administered AAV9. Mol. Ther. *21*, 1470–1471. https://doi.org/10.1038/mt.2013.95.

47. Shi, W.F., and Bartlett, J.S. (2008). Estrogen plays a critical role in AAV2-mediated gene transfer in ovarian cancer. Acta Pharmacol. Sin. *29*, 1440–1450. https://doi.org/10.1111/j.1745-7254.2008.00894.x.

48. Cabanes-Creus, M., Westhaus, A., Navarro, R.G., Baltazar, G., Zhu, E., Amaya, A.K., Liao, S.H.Y., Scott, S., Sallard, E., Dilworth, K.L., et al. (2020). Attenuation of Heparan Sulfate Proteoglycan Binding Enhances In Vivo Transduction of Human Primary Hepatocytes with AAV2. Mol. Ther. Methods Clin. Dev. *17*, 1139–1154. https://doi.org/10.1016/j.omtm.2020.05.004.

49. Milde, S., Adalbert, R., Elaman, M.H., and Coleman, M.P. (2015). Axonal transport declines with age in two distinct phases separated by a period of relative stability. Neurobiol. Aging *36*, 971–981. https://doi.org/10.1016/j.neurobiolaging.2014.09.018.

50. Sandoval, I.M., Kuhn, N.M., and Manfredsson, F.P. (2019). Multimodal Production of Adeno-Associated Virus. Methods Mol. Biol. *1937*, 101–124. https://doi.org/10.1007/978-1-4939-9065-8_6.

51. Benskey, M.J., and Manfredsson, F.P. (2016). Intraparenchymal Stereotaxic Delivery of rAAV and Special Considerations in Vector Handling. Methods Mol. Biol. *1382*, 199–215. https://doi.org/10.1007/978-1-4939-3271-9_14.

52. Sellnow, R.C., Steece-Collier, K., Altwal, F., Sandoval, I.M., Kordower, J.H., Collier, T.J., Sortwell, C.E., West, A.R., and Manfredsson, F.P. (2020). Striatal Nurr1 Facilitates the Dyskinetic State and Exacerbates Levodopa-Induced Dyskinesia in a Rat Model of Parkinson's Disease. J. Neurosci. *40*, 3675–3691. https://doi.org/10.1523/JNEUROSCI.2936-19.2020.

53. Grabinski, T.M., Kneynsberg, A., Manfredsson, F.P., and Kanaan, N.M. (2015). A Method for Combining RNAscope In Situ Hybridization with Immunohistochemistry in Thick Free-Floating Brain Sections and Primary Neuronal Cultures. PLoS One *10*, e0120120. https://doi.org/10.1371/journal.pone.0120120.

54. Steece-Collier, K., Stancati, J.A., Collier, N.J., Sandoval, I.M., Mercado, N.M., Sortwell, C.E., Collier, T.J., and Manfredsson, F.P. (2019). Genetic silencing of striatal CaV1.3 prevents and ameliorates levodopa dyskinesia. Mov. Disord. *34*, 697–707. https://doi.org/10.1002/mds.27695.